Simultaneous Measurements of Electron and Hole Sweep-Out from Quantum Wells and Modeling of Photoinduced Field Screening Dynamics

Jean Aristide Cavaillès, David A. B. Miller, *Senior Member, IEEE*, J. E. Cunningham, Patrick Li Kam Wa, and Alan Miller, *Senior Member, IEEE*

***Abstract*—We measure both electron and hole escape times from a GaAs–AlGaAs quantum well in an electric field at room temperature. This gives important information for the design of high speed quantum-well modulator and optical switching devices. The measurements are made by picosecond optical pump-probe techniques on samples containing a single quantum well in a waveguide. The use of a single well avoids multiple well transport and resonant tunneling effects. Carriers excited in the quantum well by the pump beam result in a transient bleaching signal from excitonic saturation and, as they leave the well, a transient electroabsorption signal because the movement of charge partially screens the electric field. We model both processes, including important electrical equilibration processes (such as diffusive conduction) of the sample as a whole. This modeling and the use of two samples with asymmetric barrier heights allows the measurement of the electron and hole emission as a function of applied electric field. Both electrons and holes are emitted in a few picoseconds at high fields (e.g., 100 kV/cm) in low barrier (e.g., 20% Al) structures, and in hundreds of picoseconds at low fields (e.g., 20 kV/cm) in higher barrier (e.g., 40% Al) structures. Preliminary analysis suggests that the emission mechanism is thermionic rather than by tunneling, but the results are not well explained by conventional thermionic emission models.**

I. Introduction

Electroabsorption in semiconductor multiple quantum wells (MQW) is one of the most efficient processes for making optical intensity modulators [1]–[3]. The underlying physical mechanism is the quantum confined Stark effect (QCSE) [4], by which an electric field shifts the excitonic absorption resonance towards lower photon energies. Light intensity is usually modulated by the resulting changes in absorption, and hence modulation involves the creation of electron-hole pairs inside the quantum well. These created carriers, if allowed to build up the quantum wells, tend to degrade the performance of the modulators through essentially two mechanisms: excitonic saturation and electric field screening.

Excitonic saturation is a bleaching of the exciton absorption resonance due to various many-body effects [5], [6], dominated by phase space and band filling and exchange screening [7]. The phase space and band filling are blocking mechanisms, by which carriers occupy available quantum states and inhibit further light absorption. The exchange screening changes the nature of the excitonic states, thereby changing the absorption.

Electric-field screening is itself an electroabsorption process: the photogenerated carriers screen the applied electric field, which in turn induces a change in the absorption through the QCSE. This phenomenon is particularly a problem for p-i(MQW)-n modulators, in which charge buildup inside the quantum wells due to differential escape rates between electrons and holes can lead to an inhomogeneous electric field in the intrinsic region. This can broaden the absorption edge or even inhibit the QCSE shift entirely [8]–[10].

In order to avoid these effects, one must sweep the carriers as fast as possible from the quantum well where they were created. This is even more desirable in the case of self-electrooptic-effect devices (SEED's) [11], [12], which are based on a combination of the detecting and modulating properties of p-i(MQW)-n junctions. Detection response times are ultimately limited by the speed at which the carriers can be collected, Consequently, a fast carrier sweep-out improves both the ultimate switching speed and the maximum usable intensity for SEED's.

Understanding how carriers escape from a biased quantum well is therefore important not only from a fundamental point of view, but also is an important issue in optimizing practical devices. This has motivated numerous studies [13], which have led to improvements in the design of MQW's, allowing faster switching times (down to 33 ps) for SEED's [14].

Most carrier escape time measurements so far either have concentrated on electrons or have not been able to conclude which type of carrier they were probing. Recently, however, we briefly presented the first simultaneous measurements of hole and electron escape times from biased quantum wells [15], based on pump-probe measurements on single quantum-well waveguides, with a resolution of the order of 1 ps. The only quantitative information concerning hole sweep-out from quantum wells had previously obtained by studying hole transport in MQW by time resolved photocurrent measurements

Manuscript received March 3, 1992; revised June 2, 1992. The work of P. Li Kam Wa and A. Miller was supported by DARPA.

J. A. Cavaillès is with LEP, Limeil Brèvannes, 94453 France.

D. A. B. Miller and J. E. Cunningham are with AT&T Bell Laboratories, Holmdel, NJ 07733.

P. Li Kam Wa and A. Miller are with the Center for Research in Electro-Optics and Lasers, University of Central Florida, Orlando, FL 32826.

IEEE Log Number 9202446.

0018-9197/92$03.00 © 1992 IEEE

[16], but the time resolution in this work was limited to about 100 ps. Furthermore, it was not possible in some previous studies [13] to know experimentally whether the measured times corresponded to carrier emission from one well, or included effects from multiple recapture and re-emission of carriers in subsequent wells in the multiple well samples used. The present experiments avoid this problem by using only a single well.

In this paper, we develop the concepts which have enabled us to extract electron and hole escape times from time resolved nonlinear optical transmission measurements. In particular, we give a detailed model of the dynamics of field screening by photogenerated carriers. This process is actually quite subtle, because it involves the electromagnetic properties of the sample as a whole, and a substantial part of this paper is devoted to its analysis.

The paper is organized as follows. Experimental details are given in Section II. Section III essentially describes our model of the dynamical electric field screening and how it compares with experimental results. In Section IV, we discuss the implications of our escape time measurements on the sweep-out mechanism. Our conclusions are given in Section V.

II. Experimental

A. Samples and Methods

We studied a pair of complementary samples, each containing a single GaAs-GaAlAs quantum well with asymmetric barriers, for the following reason. In a biased well, holes and electrons escape from the quantum well on opposite sides. If, for example, the quantum well is in a reverse biased p-i-n diode, electrons will leave from the side of the well facing the n-doped region and the holes from the other side. In an asymmetric well, the Al content of the barrier is different on both sides; electrons and holes have to overcome different potential barriers in order to escape from the well. Since the escape times are known [13] to depend critically upon barrier height, we expect that, at least in one of the two complementary samples, the contrast between electron and hole escape times will be enhanced with respect to what it would be in a symmetric well. This, as we will see, enables a clearer attribution of the contributions of both type of carriers to the nonlinear signal.

The structure of the samples is shown in Fig. 1. These are single mode $Ga_{0.7}Al_{0.3}As$-$Ga_{0.75}Al_{0.25}As$ double heterostructure p-i-n waveguides, with a 0.5 μm $Ga_{0.75}Al_{0.25}As$ core (where most of the light is confined). The bottom $Ga_{0.7}Al_{0.3}As$ confining layer thickness is 1 μm and the cladding layer, with the same composition, is 1.2 μm thick. The waveguide core is located in the 1 μm thick intrinsic region. The structures were grown by molecular beam epitaxy on n^+ GaAs substrates and were capped by a thin (100 Å) p^{++} GaAs layer (not shown in Fig. 1) for good ohmic contacts.

The quantum well was placed in the intrinsic region, slightly below the waveguide core, 0.17 μm above the n region. This position was chosen because it leads to a relatively small overlap between the optical mode and the quantum well (0.005). This gives a modal absorption around 60 cm^{-1} at the exciton wavelength, which enables us to work with reasonably long ($\sim$300–500 μm) samples while getting enough transmitted light, even for photon energies above the absorption edge.

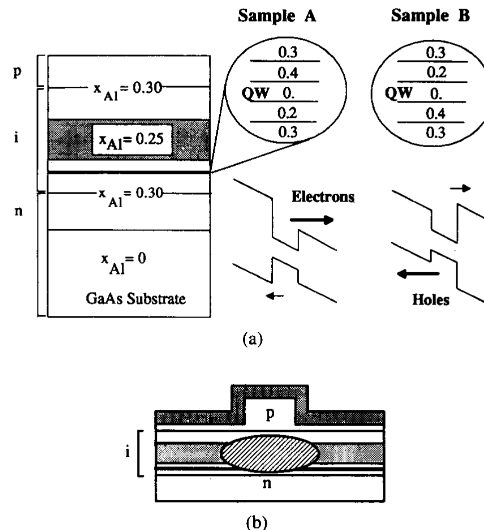

Fig. 1. (a) Schematic structure of the samples. Enlarged sections show the quantum well region for samples A and B, as well as the Al fraction of the different layers around it. The quantum wells are 95 Å thick and the $Ga_{0.6,0.8}Al_{0.4,0.2}As$ barriers are 200 Å thick. The corresponding band diagrams when the p-i-n diode is reverse biased are shown for both samples; arrows symbolize carrier escape, the longer the arrow, the faster the escape. (b) Schematic cross section of the sample. The elliptic area symbolizes the waveguide mode intensity distribution. The dotted area on top of the rib is the p-ohmic contact. (Not to scale.)

The quantum well itself consists of a 95 Å thick GaAs layer sandwiched between 200 Å thick GaAlAs barriers with a 40% Al fraction on one side and 20% on the other. For both samples, we measured similar zero-field heavy hole and light hole exciton wavelengths, around 849 and 845 nm, respectively. In sample A, the high $Ga_{0.6}Al_{0.4}As$ barrier is towards the p layer; in sample B it is on the n layer side. Under reverse bias, this leads to the band diagrams shown in Fig. 1(a). In sample A, electrons escape from the well more easily than in sample B. The situation is reversed for the holes.

Light was confined laterally using a conventional rib waveguide structure. The 4 μm wide ribs were etched chemically (0.85 μm depth) on the top surface. With this depth, the waveguide is single-moded. The ribs were clad with 30 μm wide, 0.2 μm thick Au-Zn-Au p-ohmic contact electrodes, and a AuGe-Ni-Au n-ohmic contact was deposited on the back surface of the sample. The p side was contacted using tungsten probes and the n side was glued with silver paint onto the metallic sample holder. Fig. 1(b) shows a cross section of the sample as well as the approximate intensity distribution of the guided optical mode.

We have performed pump-probe measurements using a synchronously pumped dye (Styryl9) laser tunable in the 810–880 nm range, delivering 0.7–1 ps long pulses with a 80 MHz repetition rate. In this type of experiment, one first creates electron-hole pairs in the quantum well, by absorption of a relatively intense light pulse (the pump); the changes induced by these carriers on the transmission of the sample are monitored at a later time by a weaker pulse (the probe), delayed with respect to the pump. The experimental setup is shown in Fig. 2. It is an adaptation from the one described in [13]. The output from the dye laser was actively stabilized by means of a $LiTaO_3$ electrooptic modulator connected to a feedback detector (not shown in Fig. 2). This enabled us to work at low excitation power levels while keeping a good enough signal-to-noise ratio. The pump and the probe were separated by a 50:50 beam splitter. Their polarization could be independently adjusted with $\lambda/2$ plates and polarizers. After having been delayed with respect to one another, pump and probe beams were made collinear. Light was coupled into and collected from the waveguide by means of microscope objectives. The output near-field pattern was observed using a Si CCD camera to check that the waveguides supported to a single mode. A Si p-i-n detector was used to measure output powers, with conventional lock-in techniques. The pump signal was modulated by an acoustooptic modulated at around 100 kHz.

The pump and probe beams were orthogonally polarized, so that light from the pump could be easily suppressed at the output with a polarizer. In all the experiments described here, the pump was polarized parallel to epilayers (TE) and the probe TM. The exact power coupled into the waveguide is difficult to evaluate, and it depends critically upon the position and angles of both the pump and the probe. A coupling efficiency around 20–30% was estimated by measuring the photocurrent at the excitonic resonance and assuming a unit quantum efficiency. The average optical powers coupled into the waveguide were of the order of 30 μW for the pump and 3 μW for the probe, giving a maximum photocarrier density of a few times 10^{10} cm^{-2}. We systematically checked that the signal was proportional to both the pump and probe powers, ensuring that we were in a small-signal regime.

We measured the changes in the transmission of the probe as a function of its delay relative to the pump at several wavelengths and for various biases (between +3 and −10 V). Since TM polarized light only probes optical transitions involving light holes [7], [17], we have restricted ourselves to wavelengths around the light hole exciton.

With the same setup, we also performed differential electroabsorption measurements. In these experiments, the bias is directly modulated by a small amount (± 0.1 V) around a given average value. We measure the changes in the average output power from the probe using a lock-in amplifier referenced to the modulating signal. Here again we checked that we were in a linear regime where the signal is proportional to the bias modulation amplitude.

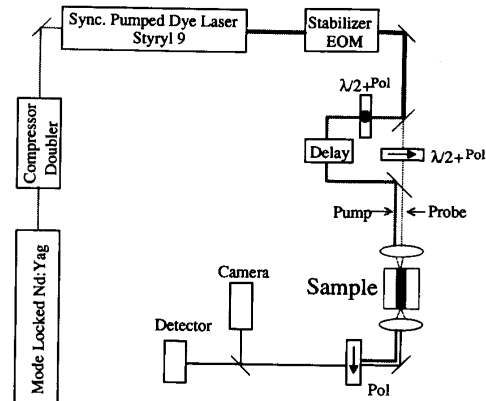

Fig. 2. Experimental setup for pump-probe measurements in waveguides.

B. Results

In our pump-probe measurements, we obtained a great variety of line shapes, depending on bias and wavelength. An example of this diversity can be seen in Fig. 3, which shows the results for both samples obtained at different wavelengths, for a 6 V reverse bias. At this bias the light hole exciton wavelength is around 855 nm. In this figure as in the following ones, a positive signal corresponds to an *increase* in transmission for the probe. The results for both samples are strikingly different.

For sample A, the sign of the signal changes with wavelength. It is positive at 859 nm and negative at 845 nm. Apart from the sign, the signal at both these wavelength shows very similar features: it rises in about 5 ps and decays with a time constant on the order of 60 ps. This wavelength sensitivity of the signal sign suggests that it primarily originates from an electroabsorption effect.

As a matter of fact, the quantum confined stark effect (QCSE) induces a strongly wavelength dependent electroabsorption [4]. For wavelengths longer than that of the excitonic resonance, an increase in the electric field across a quantum well induces an increase in absorption. Below the exciton wavelength, there is a spectral domain where an increasing field actually decreases the absorption. In fact, the wavelength at which electroabsorption changes sign is slightly longer than the exciton resonance wavelength; this is because the characteristic red shift of the absorption curves in the QCSE is actually accompanied by a broadening of the exciton resonance and a decrease in its oscillator strength. It is thus natural to conclude that the transmission changes observed for sample A at 845 and 859 nm are mainly due to an electroabsorption process induced by field screening from the photogenerated carriers. To check this hypothesis, we measured the differential electroabsorption, as explained above, and compared results with the amplitude of the pump-probe signal at different wavelengths around the light-hole exciton res-

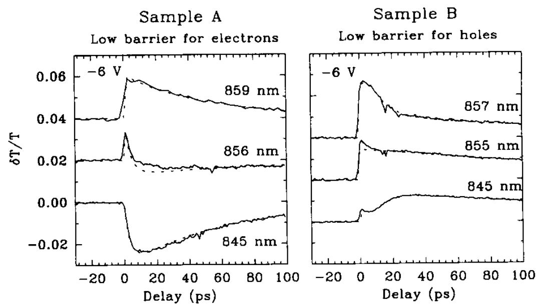

Fig. 3. Relative changes in the probe transmission induced by the pump as a function of the pump-probe delay, for both sample A and B. The reverse bias across the diodes was 6 V. The traces are recorded at the wavelengths indicated in the figure. Solid curves are experimental. Dotted curves are theoretical fits based on the analysis of Section III. Traces are offset for clarity.

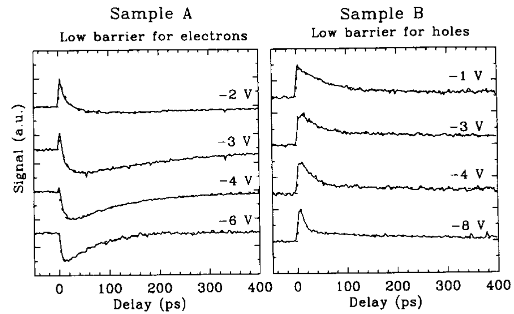

Fig. 5. Relative changes in the probe transmission induced by the pump as a function of the pump-probe delay, for both sample A and B, at different biases. Solid curves are experimental. Dotted curves are theoretical fits based on the analysis in Section III. Amplitudes are arbitrary and scales are different for each trace. Traces are offset for clarity. The wavelength was adjusted at each bias so that the electroabsorption contribution is negative for sample A and positive for sample B.

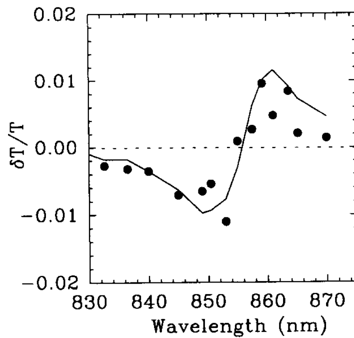

Fig. 4. Comparison of the pump probe signal amplitude (symbols) (sample A, −6 V) with directly measured differential electroabsorption (solid line). The differential electroabsorption corresponds to a 0.15 V *decrease* in the applied bias.

onance. The results are shown in Fig. 4. We see that the pump-probe signal changes sign precisely at the same wavelength as the differential electroabsorption. The sign of the differential electroabsorption spectrum shown in Fig. 4 was adjusted so that it corresponds to a decrease in the electric field (in other words it is proportional to the opposite of the derivative of the transmission with respect to the applied field). One can see that the pump-probe signal corresponds to a *decrease* in the electric field across the quantum well, as one would expect from a screening mechanism.

At −6 V, the differential electroabsorption is zero at about 856 nm. The fast signal detected at this wavelength (Fig. 3) is then primarily due to excitonic saturation. It rises instantaneously (within experimental resolution) and decays in about 5 ps. As expected, this signal corresponds to an increase in transmission.

For sample B the zero-electroabsorption wavelength (for a 6 V reverse bias) is around 855 nm. We believe the pump probe signal at this wavelength (Fig. 3) is essentially due to excitonic saturation and we observe an exponential decay with a time constant around 200 ps, as well as an instantaneous rise. Field screening manifests itself at wavelengths around 855 nm. At 857 nm, this process induces an increase in the probe transmission. This contribution thus adds to the excitonic saturation, which leads to a "bump" in the initial part of the pump-probe trace. By contrast, the field screening contribution at 845 nm induces a decrease in transmission, and is subtracted from the saturation signal. As a consequence, the pump-probe signal presents a "depression" in the first 30 ps, as one can see in Fig. 3. Note that, at 845 nm, this "dip" does not occur instantaneously, but take about 5 ps to reach a maximum (minimum in the curve).

In summary, the pump-probe signal can be described as the sum of two contributions. Excitonic saturation leads to a positive signal, at all wavelengths around the exciton. Field screening by photogenerated carriers induces a signal which changes sign with wavelength. Around the excitonic resonance wavelength, both contributions have similar amplitudes, which gives rise to complex line shapes.

We will see in Section III-B. that excitonic saturation is primarily due to the electrons. Consequently, the decay of the corresponding to the pump-probe signal gives us the electron escape time. In sample A, which has a low barrier ($Ga_{0.8}Al_{0.2}As$) for the electrons, the escape time is thus of the order of 5 ps at −6 V. In sample B, the decay is much slower (200 ps), because the electrons have a higher barrier ($Ga_{0.6}Al_{0.4}As$) to overcome.

The field screening contribution is sensitive to both electrons and holes and is much more difficult to analyse. It can be shown (see Section III-B) that the decay of this contribution is governed by the carrier with the longest escape time. Hence, the signal decay gives us the hole escape time in sample A and the electron escape time in sample B.

The wavelength dependence of the pump-probe signal described above for a −6 V bias was consistently observed for both samples for reverse biases greater than 1 V. Results at different biases are shown in Fig. 5. At each bias, the wavelength was adjusted so that the field screening contribution was negative for sample A and positive for sample B.

For sample A, the initial "spike" in the curves, which is due to excitonic saturation, tends to decay faster when the bias increases. The same is true for the decay of the field screening component, which also becomes faster at high field. This is due to the fact that the escape times of both types of carriers decrease with increasing field. The same trend is observed for sample B.

III. Theory

In this section, we describe our modeling of the experimental results, and how we can use it to deduce carrier escape times from the quantum well. We first present our analysis of the field screening process; then we introduce the excitonic saturation component and describe in detail our fitting procedure.

A. Field Screening Modeling

We assume that the changes in the transmission of the probe induced by the photocarriers are, for the field screening process, proportional to the changes in the electric field at the quantum well. (This assumption is consistent with our observation that we are in a linear regime in the experiments, with signals proportional to the excitation power.) To compute, at a given time, the variations of the electric field across the quantum well induced by the photogenerated charges, one must take into account both types of carriers and consider those that are still in the well in addition to those that have escaped from it. As a consequence, the dynamics of the carrier motion across the intrinsic region (diffusion and drift) comes into play. In addition, one must not forget the free carriers in the electrodes (doped regions of the p-i-n diode and the metallic contacts): as we will see, they react very fast to any perturbation in the electrical potential and influence the field screening process even on very short timescales [18], [19].

In this section, we will first analyze the influence of the carriers in the electrodes and then present a simple modeling of the field generated by the photocarriers.

1) Diffusive conduction: We call "diffusive conduction" the process by which carriers in the electrodes react to any localized perturbation in the electrostatic potential. The importance of this phenomenon in the context of pump-probe measurements on biased p-i(MQW)-n diodes was first realized in [18], in which it was proved to be the essential mechanism in the fast recovery of the absorption. Our discussion here follows the one in [18] and [19], adapted to the one dimensional situation of our waveguide experiments.

The main conclusion of this section is that diffusive conduction essentially locks the potential drop across the junction to its equilibrium value, on a picosecond timescale. This conclusion is based on a simple dynamic electrical model, which leads to analytical solutions and which only presumes to provide orders of magnitude.

The simplest electrical model of a p-i-n diode (and its contacts) is an array of resistors and capacitors (Fig. 6).

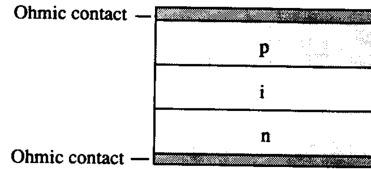

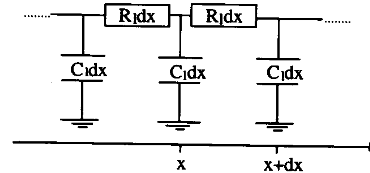

Fig. 6. Electrical circuit equivalent to a free standing p-i-n diode. R_l and C_l are unit length resistance and capacitance.

The resistances are due to the finite conductivity in the doped semiconductor and in the ohmic contacts. In Fig. 6, R_l represents the sum of the resistance per unit length of the p and n electrodes and C_l the capacitance per unit length associated with the intrinsic region. It is easy to show that the electrostatic potential $V(x, t)$ across the junction at position x and time t obeys a diffusion-like equation:

$$\frac{\partial^2 V(x, t)}{\partial x^2} = R_l C_l \frac{\partial V(x, t)}{\partial t}. \tag{1}$$

In the case of an infinite sample, a well-known solution to (1) corresponds to a Gaussian distribution, the width of which increases in time:

$$V(x, t) = \frac{K}{\sqrt{At + \Omega^2}} \exp\left(\frac{x^2}{At + \Omega^2}\right) \tag{2}$$

where $A = (2/R_l C_l)$, Ω is the initial width of the distribution and K is a multiplicative constant. Note that K is proportional to the total charge associated with the voltage perturbation, $Q = \int_{-\infty}^{+\infty} C_l V(x, t)\, dx$, which is constant throughout this spreading process. This solution shows that a perturbation in V initially localized in a region of width Ω will spread out and will eventually be canceled by the charge rearrangements inside the electrodes. This equilibration follows an inverse square root law, governed by the time constant $\tau_{hom} \equiv R_l C_l \Omega^2$. This time constant varies as the square of the lateral dimension of the initial distribution.

The discussion above is valid for a "free standing," unbiased, p-i-n junction. In the case of a biased system, one can still use an array of resistors and capacitors, but one must now take contact resistance into account. This is shown in Fig. 7, in which R_c is the unit length contact resistance ($\Omega \cdot$ cm). The total resistance of the contact is R_c divided by the contact length. The evolution equation now has the form:

$$\frac{\partial^2 V(x, t)}{\partial x^2} = R_l C_l \frac{\partial V(x, t)}{\partial t} + \frac{R_l}{R_c}(V_0 - V(x, t)). \tag{3}$$

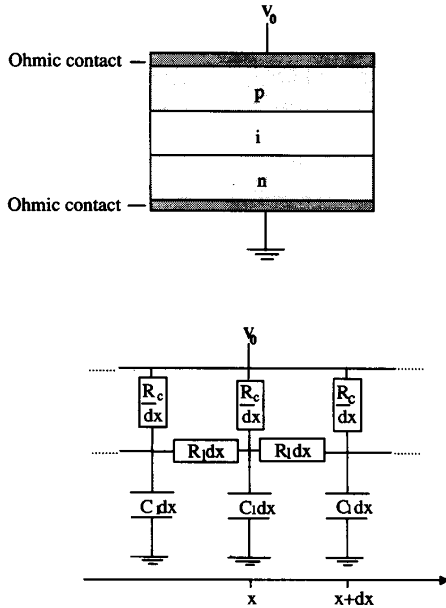

Fig. 7. Electrical circuit equivalent to a biased p-i-n diode. R_l and C_l are unit length resistance and capacitance. R_c is the unit length contact resistance.

A solution is, simply, for an applied voltage V_0;

$$V(x, t) = V_0 + \frac{K}{\sqrt{At + \Omega^2}} \exp\left(-\frac{x^2}{At + \Omega^2}\right) \times \exp\left(-\frac{t}{R_c C_l}\right). \quad (4)$$

The return to equilibrium of a biased p-i-n junction that has been locally perturbed electrically thus involves two processes with different characteristic times. The perturbation tends to become spatially uniform with the time constant τ_{hom}, and the associated charge decreases exponentially with a time constant $\tau_{dec} = R_c C_l$.

These two time constants have very different orders of magnitude. They can be easily computed from published values of electron and holes mobilities [20] and metallic conductivities. For our experimental structure (0.2 μm thick p-ohmic contact metal, 1.5 μm thick p layer and 100–300 μm thick n layer), the product $R_l C_l$ is of the order of 2.5×10^{-9} s/cm^2. Since, in our case, the perturbation is initially localized in the waveguide, one has $W \cong 2$ μm and $\tau_{hom} \cong 1 \times 10^{-4}$ ps. Assuming a pessimistic unit area contact resistance around 0.1 $\Omega \cdot$ cm^2, one finds $R_c C_l \cong 1$ ns.

Fig. 8 shows the decay of the voltage perturbation at the position where it is maximum ($x = 0$) as a function of time, for the parameters corresponding to our experimental samples. After only 0.1 ps, it has decreased by a factor of 25 with respect to its initial value. In this case, the electrostatic potential across the structure becomes uniform much more quickly than in the case of vertical incidence measurements, as those reported in [18]. This is due to the small dimensions of the exciting beam (the guided mode is only ~4 μm wide) and to the fact that the structure is capped by low resistivity metallic electrodes, which for obvious practical reasons is not the case for vertical incidence samples (where the top contact layer has to be a transparent semiconductor).

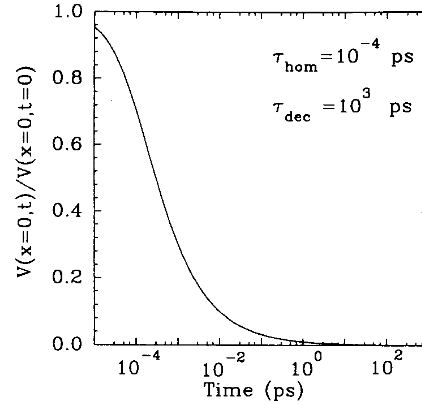

Fig. 8. Decay of the electrostatic potential across the intrinsic region at the center of the rib waveguide as a function of time, for the indicated values of the time constants τ_{hom} and τ_{dec} (see text).

The overall recharging of the structure through the contact resistance may take somewhat longer ($R_c C_l \cong 1$ ns), longer than the timescale of most of our experiments. This process, however, is fast enough that there is negligible charge (and voltage change) buildup between successive optical pulses ($\cong 10$ ns).

In conclusion, the net effect of the diffusive conduction phenomenon is to keep the potential drop across the p-i-n junction constant, *even on a picosecond timescale*:

$$V(x, t) \cong V_0 \quad (5)$$

2) Photoinduced Electric Screening: In this section, we present our computation of the variations of the electric field across the quantum well induced by the photogenerated carriers.

The geometrical parameters of the system are described in Fig. 9. In this figure, we also show schematically the charge distribution in the p-i-n intrinsic region at a given time after the excitation pulse. The charge density corresponding to the carriers in the well is approximated by Dirac distributions, i.e., "sheets" of charge. In a biased quantum well, wave functions are distorted, so that the average positions of electrons and holes are offset [4]. This is taken into account in our model by allowing for different positions for the Dirac distributions associated with the electrons and the holes. We neglect the width of the depletion layers in the p and n layers; the corresponding sheet charges are shown in Fig. 9.

We assume that the exciting pulse is instantaneous. At a time t after this pulse the density of carriers remaining

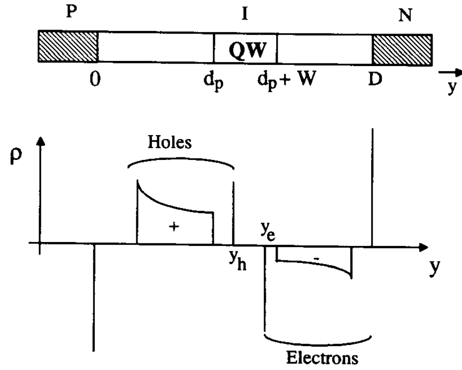

Fig. 9. Schematic charge distribution in the intrinsic region some time after excitation by the pump pulse. Carriers in the well are represented by Dirac distributors. Not to scale.

in the well is:

$$N_e = N_0 e^{-(t-\tau_e)} \quad \text{and} \quad N_h = N_0 e^{-(t/\tau_h)} \tag{6}$$

where $N_e(N_h)$ is the electron (hole) density and $\tau_e(\tau_h)$ is the electron (hole) escape time. N_0 is the initial electron-hole pair density created by the pump pulse.

We suppose that, once the carriers have left the well, they drift in the applied electric field with the saturated drift velocity v. This is valid if the electric field is greater than 10 kV/cm [20], which corresponds to a 1 V reverse bias for a 1 μm intrinsic region. In a first approximation, we neglect carrier diffusion. We assume the same drift velocity for the holes and the electrons.

Under these assumptions, it is easy to compute the space charge associated with the carriers which have left the well. One must distinguish two cases, depending whether the carriers have reached the doped regions or not. For the electrons, one has, if d_n is the well-n region distance ($d_n = D - d_p - W$)

if $t < d_n/v$ then

$$\rho_e^{esc}(y, t) = -\frac{eN_0}{v\tau_e} \times \exp\left(-\frac{vt - y - d_p - W}{v\tau_e}\right) \quad \text{if } d_p + W < y < d_p + W + vt$$

$$\rho_e^{esc}(y, t) = 0 \quad \text{elsewhere} \tag{7}$$

if $t > d_n/v$ then

$$\rho_e^{esc}(y, t) = -\frac{eN_0}{v\tau_e} \times \exp\left(-\frac{vt - y - d_p - W}{v\tau_e}\right) \quad \text{if } d_p + W < y < L'$$

$$\rho_e^{esc}(y, t) = 0 \quad \text{elsewhere.} \tag{7.1}$$

In these expressions, ρ_e^{esc} is the charge density due to the electrons that have escaped from the well, W is the well width, dp is the well-p region distance (see Fig. B1), and e is the electronic charge.

Similarly, for the holes:

if $t < d_p/v$ then

$$\rho_h^{esc}(y, t) = \frac{eN_0}{v\tau_h} \times \exp\left(-\frac{vt + y - d_p}{v\tau_h}\right) \quad \text{if } d_p - vt < y < d_p$$

$$\rho_h^{esc}(y, t) = 0 \quad \text{elsewhere} \tag{8}$$

if $t > d_p/v$ then

$$\rho_h^{esc}(y, t) = \frac{eN_0}{v\tau_h} \times \exp\left(-\frac{vt + y - d_p}{v\tau_h}\right) \quad \text{if } 0 < y < d_p$$

$$\rho_h^{esc}(y, t) = 0 \quad \text{elsewhere} \tag{8.1}$$

with obvious notations.

The photogenerated charges remaining in the well are approximated by Dirac distributions, so that, in total:

$$\rho_e(y, t) = -eN_0 e^{-(t/\tau_e)} \, \delta(y - y_e) + \rho_e^{esc}(y, t) \tag{9}$$

$$\rho_h(y, t) = eN_0 e^{-(t/\tau_h)} \, \delta(y - y_h) + \rho_h^{esc}(y, t) \tag{9.1}$$

where $y_{e(h)}$ is the position of the sheet density corresponding to the electrons (holes) remaining in the well (see Fig. 9), and $\delta(y)$ is the Dirac distribution. From the charge densities given in (9) and (9.1), one can deduce the electric field by solving Maxwell's equation:

$$\frac{\partial F(y, t)}{\partial y} = \frac{\rho_e(y, t) + \rho_h(y, t)}{\epsilon_0 \epsilon_r} \tag{10}$$

in which ϵ_0 is the vacuum permittivity and ϵ_r the dielectric constant of the intrinsic region.

Equation (10) is easy to solve. It enables us to determine the electric field distribution in the structure with an unknown integration constant.

This constant can be determined from the conclusions of the previous paragraph: the total potential drop across the intrinsic region is constant, due to diffusive conduction in the electrodes. If V_0 is the applied bias, one writes:

$$\int_0^D F(y, t) \, dy = V_0 \tag{11}$$

where D is the width of the intrinsic region. In conjunction with (10), (11) thus enables to compute $F(y, t)$ unambiguously.

The electric field induced changes in the optical properties of the quantum well are, in a first order approximation, proportional to the average value of the electric field change in the quantum well:

$$\Delta F_{QW}(t) = \frac{1}{W} \int_{dp}^{d_p + W} F(y, t) \, dy - \frac{V_0}{D} \tag{12}$$

The analytical expression of $\Delta F_{QW}(t)$ in the general case is given in Appendix A. In the following, we will analyze

some particular cases which illustrate the basic trends predicted by this model and observed in our experiments.

a) Situation where one of the carriers has an infinite escape time: In the samples studied in this paper, one type of carrier usually leaves the well much faster than the other. In this section, we will study the limiting case where one of the carrier has an infinite escape time. Let us assume, for example, that the holes have an infinite escape time. The adaptation of the results to the opposite situation (electrons with an infinite escape time) is straightforward.

We apply the general results presented in the appendix and neglect for the moment the displacements of the positive and negative charge sheets inside the well ($[\delta_e/W] \ll 1$ and $[\delta_n/W] \ll 1$); we also neglect the ratio of the well thickness to the intrinsic region width ($[W/D] \ll 1$, in our sample this ratio is 0.01). We find

$$\frac{\Delta F_{QW}}{F_0} = \frac{1}{2}\left\{(e^{-(t/\tau_e)} - 1) \times \left(1 + \frac{2v\tau_e}{D}\right) + \frac{2vt}{D}\right\} \quad \text{if } t < \frac{dn}{v} \tag{13}$$

$$= \frac{1}{2}\left\{e^{-(t/\tau_e)} \times \left(1 - \frac{2v\tau_e}{D}(e^{(dn/v\tau_e)} - 1)\right) + \frac{d_n - d_p}{D}\right\} \quad \text{if } t \geq \frac{d_n}{v} \tag{13.1}$$

where F_0 is the field that would exist between the plates of a plane capacitor with a eN_0 charge (see Appendix A, (A3)).

In Fig. 10, we plot the evolution of ΔF_{QW} as a function of the reduced time t/τ_e, for different values of the parameter $A = (2v\tau_e/D)$. The geometrical parameters used in this figure correspond to our experimental devices ($d_n/D = 0.2$, $d_p/D = 0.79$).

In all cases, the electric field tends towards a nonzero value at infinite times. This is a consquence of the fact that the well remains positively charged by the holes once all the electrons have escaped from it. The value of the limiting field change is:

$$\Delta F_\infty = \frac{F_0}{2} \times \frac{d_n - d_p}{D}. \tag{14}$$

It is interesting to note that the sign of this limit depends upon the position of the quantum well in the junction (through the difference $d_n - d_p$). This can be rationalized as follows. Due to diffusive conduction, the average value of the field in the well is adjusted so that the total potential drop across the junction remains unchanged. At very long times, the holes remaining in the well create a uniform field on each side of the well. If the well was in the center of the intrinsic region, the potential drop across the junction associated with this field would be exactly zero and the field at the well would not change.

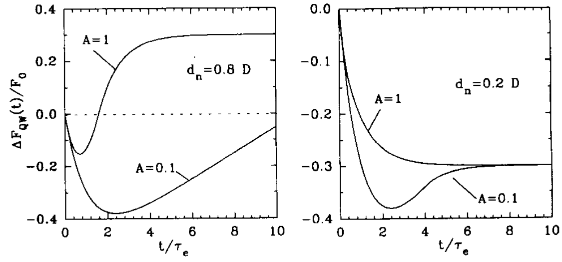

Fig. 10. Evolution of field scattering as a function of time for the indicated values of the parameter A ($= 2v\tau_e/D$) and for two different positions of the well inside the junction. d_n is the distance from the well to the n-doped region. The hole escape time is taken infinite. There is no wave function offset.

If the well is closer to the n-doped region than to the p-doped one, the potential drop across the junction associated with the field created by the holes in the well is *positive*. Through diffusive conduction, this potential drop is compensated by a decrease in the average field in the intrinsic region. Similarly, if the well is closer to the p region than the n region, the potential drop due to the holes is *negative* and is compensated by an *increase* in the average field. It may seem paradoxical that a screening phenomenon leads to an increasing field: this is a direct consequence of the diffusive conduction process. Note, however, that in the initial part of the cruves, the field change is always negative; this corresponds to a situation where some of the carriers have left the well and screen the electric field, but these carriers are still too localized in the vicinity of the well to create a substantial potential drop across the intrinsic region, so that diffusive conduction does not play any role at these early times.

The fact that the field change converges towards a finite value at infinite times is a direct consequence of our assumption that one of the carrier types (here the holes) has an infinite escape time. At very long times (compared to the electron escape time), the quantum well is electrically charged by the holes that remain in it. If the holes have a finite escape time τ_h the well will discharge itself exponentially with the same time constant, and the field change will decrease proportionally. We can thus conclude that, in general, the long term decay of the screening field component is exponential, with the time constant corresponding to the escape time of the slower carrier. (By slower, we mean here the carrier which has the longest escape time.) This point can easily be checked from the general formulas given in the Appendix.

As Fig. 10 shows, the electric field change presents, in some cases, an extremum as a function of time. It can be proved that this is always the case when $d_n > d_p$, and only for a given range of the parameter A (the details of which are not essential here) when $d_n < d_p$. Such a feature can be easily identified in an experimental pump-probe measurement and it is interesting to relate the time at which this extremum occurs to the physical parameters of the system. We find that the field change goes through an ex-

tremum at the time t_m given by:

$$t_m = \tau_e \times \log\left(1 + \frac{D}{2v\tau_e}\right). \qquad (15)$$

The time t_m is always smaller than $D/2v$, which is half the time taken by a carrier to drift across the intrinsic region.

B. Comparison with Experiments

As we have seen in the experimental section, our pump-probe measurements show contributions from both field screening by photogenerated carriers and excitonic bleaching. In the previous section, we have presented our model of the electric field changes as a function of time. A complete simulation of the experimental results also requires the computation of the exciton bleaching component.

As already mentioned, excitonic saturation at room temperature is essentially due to electrons present in the wells, and much less to the holes. This is mainly due to the fact that the density of electronic states is smaller than that of hole states. For a given carrier, the density of states close to the subband edge is proportional to its effective mass in the plane of the wells [7]. At the band edges, these effective masses, computed from a 4 band $k \cdot p$ model [21], are, if m_0 is the mass of a free electron, 0.07 $\times$ m_0 for the electrons, 0.21 $\times$ m_0 for the heavy holes, and 4 $\times$ m_0 for the light holes (for which the dispersion curve is almost flat at the top of the first level subband). As a consequence, the density of states in the valence band is much higher than in the conduction band. At room temperature, the electron gas is thus degenerate whereas the holes are not and the electronic states are much more effectively filled.

As a consequence, we assume that the pump probe signal component originating from excitonic saturation follows a simple exponential decay, with a time constant corresponding to the electrons' escape time. We thus write the pump-probe signal as:

$$\frac{\Delta T}{T}(t) = C_{sat} \times e^{-(t/\tau_e)} + C_{scr} \times \Delta F_{QW}(t) \qquad (16)$$

where $(\Delta T/T)(t)$ is the relative change in the probe transmission induced by the pump at a time t after the pump pulse, C_{sat} and C_{scr} are the amplitudes of the saturation and field screening contributions, respectively, and $\Delta F_{QW}(t)$ is the electric field variation at the quantum well (as described in the Appendix).

Fig. 11 presents a detailed comparison between an experimental result and the above theory for sample B (for which holes escape faster form the well than electrons). A very good agreement is observed for the values of the parameters indicated in the figure caption. The best fit is obtained assuming a saturated drift velocity of 7 $\times$ 10^6 cm/s, very close to the GaAs published value of 10^7 cm/s [20]. In this example, we assumed nonzero values for the

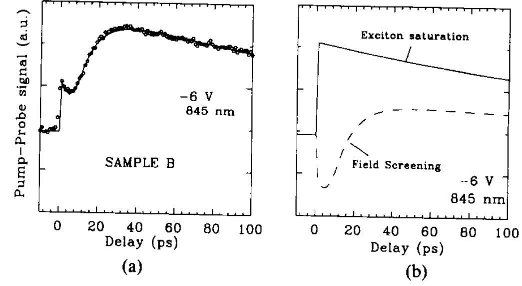

Fig. 11. (a) Fit of an experimental result with formula (18). The experiment data were taken with sample B, at −6 V and 845 nm. The parameters are: electron escape time −210 ps; hole escape time −10 ps, saturated drift velocity: 7 $\times$ 10^6 cm^{-2}, wave function offsets $\delta_e = \delta_h = 0.1 \times W$, $C_{scr} = 0.22$, $C_{sat} = 0.11$. Excitonic saturation and field screening contribution are shown in (b).

wave fuction offsets δ_e and δ_h (both are taken equal to one tenth of the well width). For a general discussion on the influence of these parameters, see Appendix B. The improvements in the fit due to this last hypothesis are, in fact, marginal. They are not significant enough to claim the observation of the instantaneous rise of the field screening component that we predicted in Section II-A. Further work, with a better time resolution (shorter pulses) should clarify that point. The accuracy on the escape times deduced from the fits is estimated to be around 10–20%.

In Fig. 11(b), we have separated the contributions due to field screening and to excitonic saturation. Note that the field screening component is positive after about 20 ps, and at longer times, decays exponentially with the same time constant as the excitonic saturation, i.e., the electronic escape time. From the value of C_{scr}, and having measured a differential electroabsorption coefficient $d(\Delta T/T)/dF$ ($\cong$ 0.005 cm/kV) at this wavelength, one can deduce the value of F_0. We find $F_0 \cong 3.6$ kV/cm, which, from (A3), corresponds to a carrier density of 2.6 $\times$ 10^{10} cm^2. This number has the expected order of magnitude for a few tens of microwatts of pump input power.

In Fig. 3, we had also presented fits of (18) to experimental data obtained at the same bias as in Fig. 11 (−6 V), but at three different wavelengths. The agreement is very good in all cases. All three experimental curves have been fitted using exactly the same set of parameters, except for the amplitudes of the screening and saturation components C_{sat} and C_{scr}. This is not surprising, since these parameters are the only ones which are wavelength sensitive. It is important to note that, in particular, the escape times giving the best fit are the same in all three cases, as they should be.

IV. Escape Time Measurements

The model described in Section III enabled us to perform the first simultaneous measurements of electron and hole escape times from a biased quantum well. We studied the influence of the electric field on these parameters for fields varying between 10 kV/cm and 100 kV/cm.

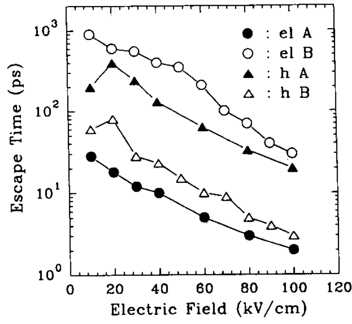

Fig. 12. Electron (circles) and hole (triangles) escape times for sample A (filled symbols) and B (open symbols), as a function of the applied electric field.

The results are shown in Fig. 12. As expected, holes escape faster from sample B than from sample A, and the contrary is true for the electrons. Similarly, holes escape faster than electrons in sample B, and slower in sample A.

For the electrons and the holes, and for both samples, the escape times decrease approximately exponentially with the applied field. The slope, in a semilog plot (Fig. 12), of the escape time versus electric field curves are remarkably similar for both samples and both types of carriers. This fact suggests, as we discussed below, that, among the two main escape mechanisms [13], thermionic emission and field-induced quantum tunneling, the first one is dominant.

For a charged paricle of mass m, the quantum tunnelling time of a quasi-bound state corresponding to an energy E across a potential barrier V in presence of an external electric field F is given by [22]:

$$\tau_T \propto \exp\left(\frac{4}{3hFe}\sqrt{2m}\,(V-E)^{3/2}\right). \tag{17}$$

This formula is in contradiction with our experimental results, on at least two points. First, if the quantum tunneling process was dominant, the escape time would depend exponentially on the *inverse* of the electric field, in contrast to the observed behavior in Fig. 12, which shows times decreasing approximately exponentially with field. Second, (17) predicts that the field dependence of the escape time is very sensitive to the mass of the particle, which we do not observe experimentally. We thus conclude that direct quantum mechanical tunneling plays little role at room temperature as far as the escape from a single quantum well is concerned. Note that this is not true in the case of multiple quantum wells, where resonant quantum tunneling has been experimentally demonstrated [23].

Thermionic emission times, on the other hand, have been calculated [13], [16] from a simple model to be

$$\tau_{th} = \left(\frac{2\pi m W^2}{kT}\right)^{1/2} \exp\left(\frac{E_b - E - F \cdot W/2}{kT}\right) \tag{18}$$

where E_b is the barrier height, as determined by the Al content of the alloy, E is the energy of the bound state we consider, and kT is the Boltzmann factor. This formula indeed predicts an exponential decrease of the escape times with field. Moreover, the slope, in a semilog plot of the escape time as a function of the field depends only upon W and not on the mass of the particle. This is consistent with Fig. 12, where the slopes of the lines are all approximately equal. Experimentally, we find a slope $s = 35 \pm 5\ 10^{-3}$ cm/kV, which is within a factor of two of the theoretical value $eW/2kT\,(= 19 \cdot 10^{-3}$ cm/kV at room temperature).

The dependence of the escape time on the barrier height that one can deduce from our measurements does not, however, correspond to what is predicted by (18). If, for example, one takes the ratio of the electron escape time for sample A (20% Al barrier) to the one for sample B (40% Al barrier), one should have, from (18):

$$\frac{\tau_e(\text{sample A})}{\tau_e(\text{sample B})} = \exp\left(\frac{E_b(A) - E_b(B)}{kT}\right) \tag{19}$$

where $E_b(A, B)$ are the barrier heights for sample A and sample B (we neglect the difference in change in the confinement energies for samples A and B). The experimental value of this ratio is about 0.03 for the electrons and 6.7 for the holes (for them, the barrier is higher in sample B than in sample A). Assuming a 67:33 value for the conduction : valence band offset ratio [24], (21) leads to a value of this ratio of 9.8×10^{-4} for the electrons and 30 for the holes. Interestingly, one can make (19) agree with the experimental values for both the electrons and the holes, if one assumes that *both types* of carriers have a temperature of 600 K.

If the experimental slope is in qualitative agreement with conventional thermionic model predictions, the absolute values of the escape times are not. For example, at -5 V, (18) leads to very small escape times for the holes (around 0.5 ps), much shorter than the measured 15 ps.

IV. Conclusion

In conclusion, we have presented a detailed analysis of the time-resolved nonlinear optical transmission measurements in biased quantum wells. In such systems, the field screening and excitonic saturation processes have comparable magnitudes, and can be clearly identified. The dynamics of the field screening process has been quantitatively analyzed, and we have shown that the diffusive conduction phenomenon plays an essential role in the process. Our model is in excellent agreement with the experimental results, in a wide range of both applied biases and wavelengths.

Electron and holes escape time from biased quantum wells have been measured simultaneously for the first time. The results suggest that the main sweep-out mechanism is of thermal origin, but the conventional models are in disagreement with our experimental findings. More experimental data are needed on different samples and at

different temperatures in order to clarify these mechanisms. The method and analysis presented here should prove a useful basis for such future studies.

Appendix I

We give here the analytical expression of the average value of the electric field in the quantum well as a function of time. We write

$$F_{QW}(t) = \frac{V_0}{D} + \Delta F_{QW}(t) \quad \text{(A1)}$$

V_0/D is the equilibrium electric field. One finds:

$$\frac{\Delta F_{QW}}{F_0} = C(t) \times \left(1 - \frac{W}{D}\right) + \frac{1}{D} \times (G_e(t) + G_h(t)) \quad \text{(A2)}$$

where:

$$F_0 = \frac{eN_0}{\epsilon_0 \epsilon_r} \quad \text{(A3)}$$

$$C(t) = e^{-(t/\tau_e)} \times \left(\frac{1}{2} - \frac{\delta_e}{W}\right) + e^{-(t/\tau_h)} \times \left(\frac{1}{2} - \frac{\delta_h}{W}\right) - 1 \quad \text{(A4)}$$

$$\delta_e = d_p + \frac{W}{2} - y_h, \quad \delta_h = y_h - \left(d_n + \frac{W}{2}\right) \quad \text{(A5)}$$

$$G_e(t) = vt + v\tau_e \times (1 - e^{-(t/\tau_e)}) \quad \text{if } t < d_n/v \quad \text{(A6)}$$

$$G_e(t) = d_n + v\tau_e e^{-(t/\tau_e)} \times (e^{(d_n/v\tau_e)} - 1) \quad \text{if } t > d_n/v \quad \text{(A6.1)}$$

$$G_h(t) = vt + v\tau_h \times (1 - e^{-(t/\tau_h)}) \quad \text{if } t < d_p/v \quad \text{(A7)}$$

$$G_h(t) = d_p + v\tau_h e^{-(t/\tau_h)} \times (e^{(d_p/v\tau_h)} - 1) \quad \text{if } t > d_p/v. \quad \text{(A7.1)}$$

In these expressions, we have introduced the quantities $\delta_{e,h}$ which represent the offset of the dirac functions corresponding to the electrons (holes) remaining in the well with respect to the center of the well.

Appendix II
Influence of the Wave Function Polarization

In a biased well, the wave functions of the holes and electrons are distorted. This was taken into account in our model by allowing for different positions of the Dirac distributions corresponding to the electrons and holes remaining in the well. The main consequence of this phenomenon is that it implies an *instantaneous* rise of the screening field component. The zero time field change is given by:

$$\Delta F_{QW}(t = 0) = -\frac{\delta_e + \delta_h}{W} \times \left(1 - \frac{W}{D}\right) \cong -\frac{\delta_e + \delta_h}{W}. \quad \text{(A8)}$$

In which $\delta_{e(h)}$ is the offset of the electrons (holes) charge densities, with respect to the center of the well [see (A5)]. A reasonable estimation for $\delta_{e(h)}$ from the electron (hole) wavefunction $\Psi_{e(h)}(y)$ is:

$$\delta_{e,h} = \int_{-\infty}^{+\infty} \Psi_{e,h}(y) y \, dy - yc \quad \text{(A9)}$$

where y_c is the position of the center of the quantum well.

The time resolution of our experiments did not actually allowed us to conclude that we have unambiguously observed this instantaneous polarisation in our measurements. This effect should be possible to measure with shorter light pulses ($\cong 100$ fs). It is also expected to be stronger in situations were the wavefunctions are easily polarizable, as is the case in coupled quantum wells, for example.

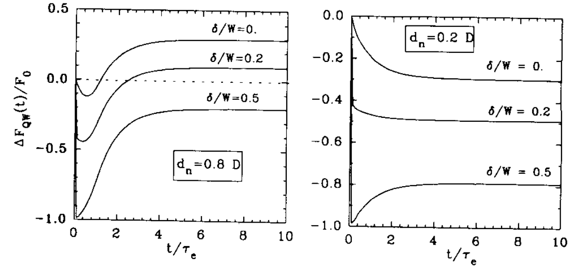

Fig. 13. Evolution of field screening as a function of time for the indicated values of the wave function offset $\delta(= \delta_e = \delta_h)$ for different positions of the well inside the junction. The parameter A $(= 2v\tau_e/D)$ is equal to 2. d_n is the distance from the well to the n-doped region.

Fig. 13 shows the time dependence of the field change, in the same hypothesis as in the previous section (infinite escape time for the holes) for various values of the wavefunction offsets and for two different positions of the quantum well inside the intrinsic region. Apart from the instantaneous rise of the field changes, the most remarkable feature of these curves is that the limit of the field changes at infinite times varies with $\delta_{e,h}$. This is due to the fact that, if the sheet charge corresponding to the holes remaining in the well is offset with respect to the center of the well, then the average value of the field it creates in the well is not equal to zero.

Acknowledgment

We gratefully acknowledge help from G. E. Doran and C. A. Burrus, as well as many stimulating discussions with J. Feldmann, T. C. Damen, I. Brener and G. D. Boyd.

References

[1] D. A. B. Miller, "Quantum wells for optical information processing," *Opt. Eng.*, vol. 26, pp. 368–372, 1987.

[2] D. A. B. Miller, J. S. Weiner, and D. S. Chemla, "Electric field dependence of linear optical properties in quantum well structures: Waveguide electroabsorption and sum rules," *IEEE J. Quantum Electron.*, vol. QE-22, pp. 1816–1830, 1986.

[3] G. D. Boyd, D. A. B. Miller, D. S. Chemla, S. L. McCall, A. C. Gossard, and J. H. English, "Multiple quantum well reflection modulator," *Appl. Phys. Lett.*, vol. 50, pp. 1119–1121, 1987.

[4] D. A. B. Miller, D. S. Chemla, T. C. Damen, A. C. Gossard, W. Wiegmann, T. H. Wood, and C. A. Burrus, "Electric field dependence of optical absorption near the bandgap of semiconductor structures," *Phys. Rev. B*, vol. 32, pp. 1043–1060, 1985.

[5] D. S. Chemla and D. A. B. Miller, "Room temperature excitonic nonlinear-optical effects in semiconductor quantum well structures," *J. Opt. Soc. Amer. B*, vol. 2, pp. 1155–1173, 1985.

[6] H. Haug and S. Schmitt-Rink, "Basic mechanisms of the optical nonlinearities of semiconductors near the band edge," *J. Opt. Soc. Amer. B*, vol. 2, pp. 1135–1142, 1985.

[7] S. Schmitt-Rink, D. S. Chemla, and D. A. B. Miller, "Linear and non-linear optical properties of semiconductor quantum wells," *Advances in Physics*, vol. 38, no. 2, pp. 89–188, 1989.

[8] I. Bar-Joseph, G. Sucha, D. A. B. Miller, D. S. Chemla, B. I. Miller, and U. Koren, "Self electro-optic device and modulation converter with GaInAsP/InP multiple quantum wells," *Appl. Phys. Lett.*, vol. 52, pp. 51–53, 1988.

[9] T. H. Wood, J. Z. Pastalan, C. A. Burrus, Jr., B. C. Johnson, B. I. Miller, J. L. de Miguel, U. Koren, and M. G. Young, "Electric field screening by photogenerated holes in multiple quantum wells: A new mechanism for absorption saturation," *Appl. Phys. Lett.*, vol. 57, p. 1081, 1990.

[10] R. Sauer, K. Thornke, and W. T. Tsang, "Photoinduced space-charge build up by asymmetric electron and hole tunneling in coupled quantum wells," *Phys. Rev. Lett.*, vol. 61, pp. 609–612, 1988.

[11] D. A. B. Miller, D. S. Chemla, T. C. Damen, A. C. Gossard, W. Wiegmann, T. H. Wood, and C. A. Burrus, "Novel hybrid optically bistable switch: The quantum well self electro-optic effect device," *Appl. Phys. Lett.*, vol. 45, pp. 13–15, 1984.

[12] D. A. B. Miller, "Quantum well self electro-optic-effect devices," *Opt. Quantum Electron.*, vol. 22, pp. S61–S98, 1990.

[13] For a recent review see A. M. Fox, D. A. B. Miller, G. Livescu, J. E. Cunningham, and W. Y. Jan, "Quantum well carrier sweep out: Relation to electroabsorption and exciton saturation," *IEEE J. Quantum Electron.*, vol. 27, pp. 2281–2295, 1991.

[14] G. D. Boyd, A. M. Fox, and D. A. B. Miller, "33 ps optical switching of symmetric self electro optic effect devices," *Appl. Phys. Lett.*, vol. 57, pp. 1843–1845, 1991.

[15] J. A. Cavaillès, D. A. B. Miller, J. E. Cunningham, P. Li Kam Wa, and A. Miller, "Simultaneous measurement of electron and hole escape times from biased quantum wells," submitted to *Appl. Phys. Lett.*, 1992.

[16] H. Schneider and K. v. Klitzing, "Thermionic emission and Gaussian transport in a GaAs/Al_xGa_{1-x}As multiple-quantum-well structure," *Phys. Rev. B*, vol. 38, pp. 6160–6165, 1988.

[17] J. S. Weiner, D. S. Chemla, D. A. B. Miller, H. A. Haus, A. C. Gossard, W. Wiegmann, and C. A. Burrus, "Highly anisotropic optical properties of single quantum well waveguides," *Appl. Phys. Lett.*, vol. 47, no. 7, pp. 664–667, 1985.

[18] G. Livescu, D. A. B. Miller, T. Sizer, D. J. Burrows, J. E. Cunningham, A. C. Gossard, and J. H. English, "High-speed absorption recovery in quantum well diodes by diffusive electrical conduction," *Appl. Phys. Lett.*, vol. 54, pp. 748–750, 1989.

[19] G. Livescu, A. M. Fox, D. A. B. Miller, T. Sizer, W. H. Knox, J. E. Cunningham, A. C. Gossard, and J. H. English, "Optical detection of resonant tunnelling of electrons in quantum wells," *Semicond. Sci. Technol.*, vol. 5, pp. 549–556, 1990.

[20] Landolt-Börnstein, *Numerical Data and Functional Relationships in Science and Technology*, Group III, vol. 17, Subvol. New York: Springer-Verlag, 1982, pp. 218–257.

[21] I. Brener, private communication.

[22] L. D. Landau and E. M. Lifschitz, *Quantum Mechanics (Non-relativistic theory)*. New York: Pergamon, 1977, pp. 181–182.

[23] G. Livescu, A. M. Fox, D. A. B. Miller, T. Sizer, W. H. Knox, A. C. Gossard, and J. H. English, "Resonantly enhanced electron tunnelling rates in quantum wells," *Phys. Rev. Lett.*, vol. 63, no. 4, pp. 438–440, 1989.

[24] K. J. Moore, P. D. Dawson, and C. T. Foxon, "Effects of electronic coupling on the band alignment of thin GaAs/GaAlAs quantum well structures," *Phys. Rev. B*, vol. 38, pp. 3368–3374, 1988.

Jean Aristide Cavaillès was born in December 1960 in Carpentras, France. He became Professeur Agrégé in physics in 1982 and graduated from the Ecole Normale Supèrieure de Saint Cloud in 1983. He received the doctoral thesis in solid state physics from the University Paris-Xi in 1984.

After having lectured physics for two years at the WUHAN University, People's Republic of China, he joined the 'Laboratoires d'Electronique Phillips', Exploratory Research Department, Paris, in 1986. There, his work focused on the physics and applications of guided wave optics, with a particular interest for quantum confined systems. In 1991, he visited for one year AT&T Bell Labs, Holmdel, NJ, in D. A. B. Miller's Department. In March 1992 he joined the optoelectronics division at Alcatel Alsthom Research.

David A. B. Miller (M'84–SM'89), for a photograph and biography see p. 1553 of the June 1992 issue of the JOURNAL.

J. E. Cunningham was born in Oak Ridge, TN, on November 30, 1949. He received the B.Sc. degree from the University of Tennessee in 1972 and the Ph.D. degree in 1979 from the University of Illinois.

He remained at the University of Illinois as a Senior Research Physicist and worked on molecular beam epitaxy of metallic superlattices as well as the optical properties of surfaces. Since joining AT&T Bell Laboratories, Holmdel, NJ, as a member of the Technical Staff in 1985, he has investigated compound semiconductor growth using gaseous sources.

Dr. Cunningham is a member of the American Physical Society.

Patrick Li Kam Wa, for a photograph and biography see p. 874 of the April 1992 issue of this JOURNAL.

Alan Miller (M'89–SM'90) was born in Dunfermline, Scotland, on June 5, 1949. He received the B.Sc. degree in physics from the University of Edinburgh, Scotland, in 1971 and the Ph.D. degree from the University of Bath, England, in 1975. His thesis work was on the optical and electronic properties of chalcopyright semiconductors. Post-Doctoral research from 1974 to 1979 at Herlot-Watt University, Edinburgh, included the optical properties of ordered vacancy semiconductors as well as band-gap resonant optical nonlinearities and two photon absorption in semiconductors.

As a visiting Assistant Professor at North Texas State University between 1979 and 1981 he researched ultrafast phenomena in germanium including carrier cooling and anisotropic state filling. From 1981 to 1989 he worked at the Royal Signals and Radar Establishment, Malvern, England, where he headed a research group investigating optical nonlinearities in semiconductors and liquid crystals, optical bistbility, phase conjugation, self-focusing, and picosecond phenomena for applications in signal processing and optical limiting. He took up his present position as a Professor of physics and electrical engineering at the Center for Research in Electro Optics and Lasers (CREOL) at the University of Central Florida in January 1989 where he is researching new femtosecond laser sources, ultrafast phenomena in semiconductors, carrier transport phenomena in multiple quantum wells, and optical nonlinearities and switching in low-dimensional semiconductor materials and devices.

Dr. Miller is a Fellow of the Institute of Physics (UK). He received the 1991 IEEE Orlando Section Outstanding Chapter Chairman award for LEOS.